Photoelectron momentum distributions of atomic and molecular systems in strong circularly or elliptically polarized laser fields

Pei-Lun He,[1,2] Norio Takemoto,[3] and Feng He[1,4,5,*]

[1]*Key Laboratory for Laser Plasmas (Ministry of Education) and Department of Physics and Astronomy, Shanghai Jiao Tong University, Shanghai 200240, China*

[2]*School of Agriculture and Biology, Shanghai Jiao Tong University, Shanghai 200240, China*

[3]*Max-Planck-Institut für Physik komplexer Systeme, Nöthnitzer Straße 38, D-01187 Dresden, Germany*

[4]*IFSA Collaborative Innovation Center, Shanghai Jiao Tong University, Shanghai 200240, China*

[5]*State Key Laboratory of Precision Spectroscopy, East China Normal University, Shanghai 200062, China*

(Received 19 December 2014; published 19 June 2015)

Photoelectron momentum distributions of a hydrogen atom in an elliptically polarized laser field and a hydrogen molecular ion in a circularly polarized laser field are studied by simulating the time-dependent Schrödinger equation. We demonstrate that, in both systems, the Coulomb interaction between a liberated electron and its parent ion is essential for the photoelectron momentum angular drift in a laser polarization plane. By decomposing the wave packet into the rescattered and directly ionized components in the case of a hydrogen molecular ion, we reveal that the rescattered component drifts by a larger angle. The drift angle of the photoelectron of the hydrogen atom decreases monotonically with longer wavelength, while a nonmonotonic dependence is shown for H_2^+. We attribute such nonmonotonicity to the fluctuation of the instant of ionization for H_2^+ as the laser wavelength is changed.

DOI: 10.1103/PhysRevA.91.063413 PACS number(s): 32.80.Rm, 42.65.Ky, 32.30.Jc, 34.80.Qb

I. INTRODUCTION

Understanding the ionization process in intense laser fields is of central importance in ultrafast atomic, molecular, and optical sciences. Many ultrafast measurement techniques are based on the ionization and subsequently induced processes. Such techniques include the phase meter [1], ultrafast streaking camera [2–4], attoclock [5], quantitative rescattering theory [6,7], and molecular-orbital imaging [8,9], to name several examples out of many [10]. More accurate and precise understanding of the ionization process will lead to new types of measurement and control methods for the electron dynamics on attosecond time scale.

A versatile understanding of intense-field ionization has so far been achieved with several key approximation approaches. One approach is to combine the quasistatic tunnel ionization (QSTI) rate [11–14] with the classical-mechanical trajectories of a liberated electron [15–17]. This approach, which we refer to as the simple quasiclassical (SQC) model in this article but has also been known as the simple-man model [15], gives us much intuition because these trajectories can be calculated analytically by neglecting the Coulomb potential of the parent ion and taking into account only the laser-electron interaction. Another approach, based entirely on quantum mechanics, approximates the ionization as the transition from a field-free bound state to a laser-dressed continuum state [18–22]. In this approach, often referred to as the strong-field approximation (SFA), the interaction of an electron with its parent ion is neglected compared to the interaction with an intense laser field in the final continuum state, in much the same spirit as the SQC model, and this allows us to express the transition amplitude in a closed form. While these approaches have made analysis and understanding of many phenomena possible, there are naturally other phenomena that cannot be reproduced successfully by them and require refined treatments [23–30].

Ionization of atoms by an elliptically polarized (EP) laser field is an example that lies beyond the limit of applicability of the above-mentioned approximations. The SQC model and the SFA predict that the photoelectron momentum distribution (PMD) would be peaked in the direction perpendicular to the major polarization axis of the laser electric field (i.e., in the direction of the minor polarization axis). This is because the ionization rate is highest, according to the QSTI picture, when the electric field of the EP laser light takes the largest magnitude, i.e., when the rotating electric field is parallel to the major polarization axis. The photoelectron released at this instant would gain the momentum along the laser vector potential at the instant of ionization from the laser field if there were no Coulomb potential of the parent ion. If we also neglect the initial momentum, as is often done in the SQC model, the asymptotic photoelectron momentum would point in the direction of the minor polarization axis. However, observed PMDs show peaks rotated away from the predicted direction [31–43].

Ionization of molecules in a circularly polarized (CP) laser field has also shown a similar deviation from the predictions of the SQC model and SFA [30,44–53]. In this system, the ionization rate is considered to be the highest when the rotating laser electric field is parallel to the molecular axis. Therefore, the PMD is expected to have peaks in the direction perpendicular to the molecular axis.

These deviations in the PMDs from the expectation have been investigated for atomic systems and molecular systems separately. Therefore, it is not very clear whether the deviations can be explained by a common mechanism. On the one hand, it was pointed out that the Coulomb interaction between the electron and the parent ion after ionization is responsible for the deviation in atomic [32–36,38–41,43] as well as molecular systems [46–53]. Hence, the deviations, which break the fourfold symmetry of the PMD expected by the SFA, are sometimes called Coulomb asymmetry. On the other hand,

*fhe@sjtu.edu.cn

the multicenter character and the nuclear motion of molecules generally have been known to induce unique phenomena absent in atomic systems [54–71]. In fact, in studies of H_2^+, it has been pointed out that the electron wave packet does not leave the parent ion when the electric field is parallel to the molecular axis, as expected by the QSTI picture, but at a delayed timing [44,46], and that the wave packet has a non-negligible initial flow velocity [44,46,48]. These effects, originating from the bound electron dynamics prior to ionization [65–68], are considered to be specific to the molecular systems. For multielectron systems, it has been pointed out that the interaction of the photoelectron with the laser-induced dipole of the parent ion also influences the PMD [30,38,41,50].

In this paper we study theoretically the ionization of H in an EP laser field and H_2^+ in a CP laser field. We aim at clarifying what is a common mechanism to both of these single-electron systems and what is specific to each system. For this purpose, we perform sequences of numerical simulations on quantum-mechanical models by changing the model parameters systematically. The current study, based entirely on the exact solution of the quantum-mechanical (reduced-dimensional) models, avoids possible arguments about determining the initial time, position, and momentum of the classical-mechanical trajectories of the photoelectron [30,34,36,38,41,46,49,50]. At the same time, we can still extract insightful information from the sequence of simulation results with different model parameters. More precisely, by artificially screening the Coulomb potential of the parent ion at different ranges, we demonstrate that the Coulomb interaction at a relatively close range (about 10–15 a.u. from the center of the parent ion) is essential for the rotation of the PMD from the prediction of the SFA in both atomic and molecular systems. Furthermore, we introduce a method to decompose the electronic wave packet leaving the parent ion into the directly ionized component and rescattered component by applying two mask functions on the wave function, and we identify that the rescattered component is rotated by a larger angle than the direct ionization in the case of H_2^+. Finally, we calculate the drift angle from the SFA expectation by changing the laser intensity and wavelength. We show that the drift angle depends nonmonotonically on the laser wavelength in the case of H_2^+, in contrast to the monotonic dependence in the case of H atom. We relate this nonmonotonic dependence to the fluctuation of the instant of the maximum ionization rate for H_2^+ with respect to that for the H atom as the laser wavelength is changed.

In this paper we focus on the comparison of atomic and molecular systems at the simplest settings. We use the single-electron atom and molecule, and we apply the EP laser field to the atom and CP laser field to the molecule because these are the simplest fields to cause the angular deviation of the PMD in the respective systems. We use two-dimensional (2D) models of the atom and molecule, and we investigate the molecular model at the specific internuclear distance where the tunneling character is very clear. We set the laser wavelength in the near-infrared to midinfrared region, where the angular deviation has been studied in several experiments. In this way, we mainly restrict our parameter domain around the simplest conditions and perform systematic research in order to draw a unified perspective within this domain. We also extend discussions into other parameter domains, such as to multielectron systems [30,38,41,50], the different geometry of the molecule with respect to the laser field [69], and the shorter laser wavelength of the XUV to the x-ray range [51,53].

The rest of the paper is organized as follows. In Sec. II we introduce our model systems and numerical simulation methods. Section III presents a discussion based on the numerical simulation results as well as prospects for extending the present understanding to other regimes of atomic, molecular, and laser parameters. Section IV summarizes the paper.

II. MODELS AND METHODS

A. Model Hamiltonian

We used 2D models for the motion of the electron in H and H_2^+ in the laser polarization plane. For H_2^+ we aligned the molecular axis on the laser polarization plane, and we froze the nuclear motion and considered only the electronic dynamics. These reduced-dimensional models have been known to reproduce at least the main features of the experimentally observed PMD on the laser polarization plane [44,47,53]. Restricting the electronic motion on the 2D laser polarization plane may be justified since the photoelectron momentum component perpendicular to this plane has been observed to be relatively small compared to those parallel with the plane [31,45,72]. The nuclear dynamics may be considered to be effectively separated from the electronic dynamics since the observed PMDs of H_2^+ and D_2^+ had little difference between each other [47]. In the following, we set the 2D coordinates (x,y) so that the x axis is along the major polarization axis of the laser electric field in the H model and along the molecular axis in the H_2^+ model.

The Hamiltonian of the models is given by (atomic units are used throughout this article unless otherwise stated)

$$H(t) = H_0 + V_{\rm L}(t) \tag{1}$$

as a sum of the field-free Hamiltonian H_0 and the laser-electron interaction $V_{\rm L}(t)$. The field-free Hamiltonian is expressed as

$$H_0 = \frac{p_x^2}{2} + \frac{p_y^2}{2} + V_{\rm C}(x,y), \tag{2}$$

where (p_x,p_y) are the (x,y) components of the electron momentum $\mathbf{p}$, and $V_{\rm C}(x,y)$ is the Coulomb interaction between the nucleus (nuclei) and the electron. The laser-electron interaction is expressed in the velocity gauge as

$$V_{\rm L}(t) = \mathbf{A}(t)\cdot\mathbf{p} + \frac{\mathbf{A}^2(t)}{2}, \tag{3}$$

where $\mathbf{A}(t)$ is the vector potential of the laser field.

The Coulomb interaction $V_{\rm C}(x,y)$ is expressed by the soft-core potentials $V_{\rm C,H}(x,y)$ and $V_{\rm C,H_2^+}(x,y)$ in the respective cases of H and H_2^+,

$$V_{\rm C,H}(x,y) = -\frac{1}{\sqrt{x^2+y^2+\alpha}}, \tag{4}$$

$$V_{\rm C,H_2^+}(x,y) = -\sum_{s=\pm1}\frac{1}{\sqrt{[x+s(R/2)]^2+y^2+\alpha}}. \tag{5}$$

We set the soft-core parameter as $\alpha = 0.64$ a.u. We fix the internuclear distance at $R = 5$ a.u., taking into account the following factors: that H_2^+ is ionized mainly on its way to dissociation when the internuclear distance stretches to around 5–10 a.u. [64], and that the discrepancy between the PMD of the 2D model of H_2^+ and that of experiment is known to become noticeably larger from about $R > 7$ a.u. [44].

We used a four-cycle laser pulse with the electric field

$$\mathbf{E}(t) = E_0[\cos(\omega t)\hat{\mathbf{x}} - \epsilon \sin(\omega t)\hat{\mathbf{y}}]\cos^2\left(\frac{\pi t}{4T}\right) \tag{6}$$

for $t \in [-2T, 2T]$, and $\mathbf{E}(t) = \mathbf{0}$ for $t \notin [-2T, 2T]$. Here $\hat{\mathbf{x}}$ and $\hat{\mathbf{y}}$ are the unit vectors along the x and y directions, respectively. We denote the angular frequency of the laser field by ω and the laser optical period by $T = 2\pi/\omega$. We denote by ϵ the ellipticity. We applied an EP field ($\epsilon = 0.6$) to H and a CP field ($\epsilon = 1.0$) to H_2^+. The same EP field is also applied on H_2^+ when we discuss the dependence of the PMD on the molecular alignment. The laser vector potential $\mathbf{A}(t)$ in Eq. (3) is

$$\mathbf{A}(t) = -\int_{-2T}^{t} dt' \mathbf{E}(t'). \tag{7}$$

B. Wave-packet propagation

We propagated the electronic wave packet $|\Psi(t)\rangle$ from $t = t_i = -2T$ (i.e., the beginning of the laser pulse) to $t = t_f = 12T$ (i.e., ten cycles after the end of the laser pulse). The initial state $|\Psi(t_i)\rangle$ was set as the ground state $|\Phi_0\rangle$ of the field-free Hamiltonian H_0.

The time evolution of the wave packet was calculated according to the equation [73,74]

$$|\Psi(t)\rangle = |\Phi(t)\rangle - i\int_{t_i}^{t} d\tau U(t,\tau)V_L(\tau)|\Phi(\tau)\rangle, \tag{8}$$

where $|\Phi(t)\rangle$ and $|\Phi(\tau)\rangle$ are the reference parts of the wave packet defined as

$$|\Phi(t)\rangle = \exp[-iH_0(t - t_i)]|\Phi_0\rangle, \tag{9}$$

and $U(t,\tau)$ is the propagator defined as

$$U(t,\tau) = \mathcal{T}\exp\left(-i\int_{\tau}^{t} H(t')dt'\right), \tag{10}$$

with the formal time-ordering operator $\mathcal{T}$. Note that Eq. (8) is equivalent to the time-dependent Schrödinger equation

$$i\frac{\partial}{\partial t}|\Psi(t)\rangle = H(t)|\Psi(t)\rangle \tag{11}$$

with the initial condition $|\Psi(t_i)\rangle = |\Phi_0\rangle$ [75].

For numerical computations, the integral over τ in Eq. (8) was approximated by a discrete sum over the temporal grid points. At the same time, the formal propagator $U(t,\tau)$ was decomposed to a product of short-time propagators over the same grid. We set the temporal grid points, commonly for t and τ, as

$$t_l = l\Delta t + t_i, \quad l = 0, \ldots, N, \tag{12}$$

where $\Delta t = 0.05$ a.u. and $N = (t_f - t_i)/\Delta t$. Then the time evolution of the wave packet can be expressed as

$$|\Psi(t_l)\rangle \approx |\Phi(t_l)\rangle - i\Delta t\sum_{n=0}^{l-1}\bar{U}(t_l,t_n)V_L(t_n)|\Phi(t_n)\rangle, \tag{13}$$

where

$$\bar{U}(t_l,t_n) = u(t_l,t_{l-1})\cdots u(t_{n+2},t_{n+1})u(t_{n+1},t_n), \tag{14}$$

and

$$u(t_{k+1},t_k) = \exp\left[-i\Delta t H\left(t_k + \frac{\Delta t}{2}\right)\right] \tag{15}$$

for $k = 0, \ldots, N-1$. In our numerical implementation, we propagated the second term in Eq. (13)

$$|\Psi_L(t_l)\rangle := -i\Delta t\sum_{n=0}^{l-1}\bar{U}(t_l,t_n)V_L(t_n)|\Phi(t_n)\rangle, \tag{16}$$

according to the recursion relation

$$|\Psi_L(t_l)\rangle = u(t_l,t_{l-1})[|\Psi_L(t_{l-1})\rangle - i\Delta t V_L(t_{l-1})|\Phi(t_{l-1})\rangle], \tag{17}$$

with the initial condition $|\Psi_L(t_i)\rangle = 0$.

We discretized the spatial coordinates x and y by the grid points extending over $x \in [-500,500]$ a.u. and $y \in [-500,500]$ a.u. at regular intervals of $\Delta x = \Delta y = 0.2$ a.u. On this grid, the operation of each short-time propagator $u(t_{k+1},t_k)$ was approximated by the Fourier-grid Hamiltonian split-operator method [76–78].

At the end of the propagation, the ionization part was recorded as $[1 - M(r_b)]|\Psi(t_f)\rangle$, where the mask $M(r_b)$ is expressed in the (x,y) space as

$$M(r_b) = \begin{cases} 1 & \text{for } r \leqslant r_b \\ \exp[-\beta(r - r_b)] & \text{for } r > r_b, \end{cases} \tag{18}$$

where $r = \sqrt{x^2 + y^2}$, $\beta = 1.0$ a.u., and we set $r_b = 30$ a.u. We Fourier transformed the ionized wave function to obtain the PMD $|\tilde{\Psi}(\mathbf{p})|^2$. As mentioned earlier, we propagated the wave packet for $10T$ after the end of the laser pulse in order to wait for all ionized components to enter the area $r > r_b$. This also reduced the error in the PMD due to projecting the final wave packet onto plane waves instead of continuum eigenstates of H_0. We checked that the PMDs were converged with respect to the final time t_f.

C. Screening Coulomb potentials

To quantitatively investigate the effect of the long-range part of the Coulomb interaction $V_C(x,y)$ on final photoelectron momenta, we used screened Coulomb potentials in some of our simulations (i.e., those shown in Fig. 1). The screened potentials are defined as

$$V_{SC}(x,y;r_0) = V_C(x,y)M(r_0), \tag{19}$$

with the mask function M defined in Eq. (18). We carried out simulations by changing the cutoff radius r_0. It should be noted that we screened the Coulomb potential only

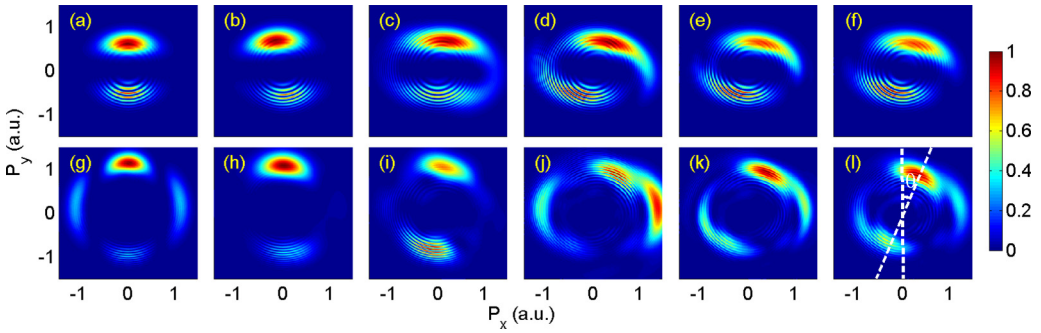

FIG. 1. (Color online) The PMDs for (a)–(f) H and (g)–(l) H_2^+ models with screened Coulomb potentials. The distributions are normalized so that the maximum value in each panel is equal to unity for better comparison. (a) and (g) The Coulomb potentials are completely neglected. (b)–(f) The cutoff radii were set as $r_0 = 2, 6, 10, 15$, and 100 a.u., respectively. (h)–(l) The cutoff radii were set as $r_0 = 3, 4, 10, 15$, and 100 a.u., respectively. The laser intensity was set at 1×10^{14} W/cm^2, and the wavelength was 800 nm for all the simulations in this figure. (a)–(f) The major axis of the polarization ellipse is along the x axis. (g)–(l) The molecular axis is along the x axis. The angle θ in (l) is used to quantify PMDs.

after the interaction with laser fields. In other words, $V_{\rm SC}$ was incorporated in the propagation described by Eq. (13) only through $\bar{U}$ but not through $|\Phi\rangle$. More precisely, the Hamiltonian operator $H(t)$ in each short-time propagator in Eq. (15) was replaced by

$$H_{\rm S}(t) = \frac{p_x^2}{2} + \frac{p_y^2}{2} + V_{\rm SC}(x,y;r_0) + V_{\rm L}(t), \qquad (20)$$

while the reference Hamiltonian H_0 in Eq. (9) retained the original potential $V_{\rm C}$. In addition, we also performed simulations by completely screening the Coulomb potentials, i.e., by setting $V_{\rm C} = 0$ in $\bar{U}$. In this case, the present simulation becomes equivalent to the SFA [75]. It should be noted that the sequence of simulations connecting the limits of the SFA and the original Coulomb interaction was made possible by using the integral equation (8) instead of the time-dependent Schrödinger equation (11).

D. Direct and rescattering ionization

It is expected that Coulomb potentials have different effects on direct and rescattering ionization. We distinguish these two scenarios as schematically illustrated in Fig. 2. Here we introduce two radial boundaries $r_{\rm d}$ and $r_{\rm s}$ ($r_{\rm s} < r_{\rm d}$). We define the direct ionization component as the wave packets that never return to the region $r < r_{\rm s}$ after they enter the region $r > r_{\rm d}$ once, e.g., as illustrated by the red solid arrow in Fig. 2. In contrast, if wave packets follow paths such as the blue dashed arrow in Fig. 2, i.e., if the wave packets first enter the region $r > r_{\rm d}$, later return to the area $r < r_{\rm s}$ at least one time, and finally escape, we assign these parts as the rescattering ionization component.

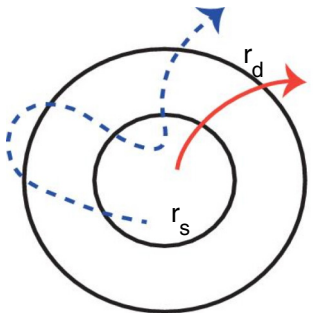

FIG. 2. (Color online) Sketch of possible paths for direct ionization (red solid arrow) and rescattering ionization (blue dashed arrow) components of the wave packet. Two boundaries $r_{\rm d} = 8$ a.u. and $r_{\rm s} = 5$ a.u. were used for the decomposition.

Numerically, we decomposed $|\Psi_{\rm L}(t_l)\rangle$ defined in Eq. (16) into the direct ionization component $|\Psi_{\rm d}(t_l)\rangle$, the rescattered component $|\Psi_{\rm r}(t_l)\rangle$, and the rest $|\Psi_{\rm ion}(t_l)\rangle$. These components were propagated and reorganized at each time step according to the following algorithm:

(1) *Initial conditions*. At the initial time $t_{\rm i}(=t_0)$, the components are set as

$$|\Psi_{\rm ion}(t_{\rm i})\rangle = 0, \qquad (21)$$

$$|\Psi_{\rm d}(t_{\rm i})\rangle = 0, \qquad (22)$$

$$|\Psi_{\rm r}(t_{\rm i})\rangle = 0. \qquad (23)$$

(2) *Propagation*. Each component is propagated by one time step as

$$|\Psi'_{\rm ion}(t_l)\rangle = u(t_l,t_{l-1})[|\Psi_{\rm ion}(t_{l-1})\rangle - i\,\Delta t\, V_{\rm L}(t_{l-1})|\Phi(t_{l-1})\rangle], \qquad (24)$$

$$|\Psi'_{\rm d}(t_l)\rangle = u(t_l,t_{l-1})|\Psi_{\rm d}(t_{l-1})\rangle, \qquad (25)$$

$$|\Psi'_{\rm r}(t_l)\rangle = u(t_l,t_{l-1})|\Psi_{\rm r}(t_{l-1})\rangle. \qquad (26)$$

(3) *Component reorganization*. At each time step, the transfer from one component to another is calculated with the mask functions in the form of Eq. (18) as

$$|\Delta\Psi_{\rm d}(t_l)\rangle = [1 - M(r_d)]|\Psi'_{\rm ion}(t_l)\rangle, \qquad (27)$$

$$|\Delta\Psi_{\rm r}(t_l)\rangle = M(r_s)|\Psi'_{\rm d}(t_l)\rangle. \qquad (28)$$

Then the components are updated as

$$|\Psi_{\rm ion}(t_l)\rangle = |\Psi'_{\rm ion}(t_l)\rangle - |\Delta\Psi_{\rm d}(t_l)\rangle, \qquad (29)$$

$$|\Psi_{\rm d}(t_l)\rangle = |\Psi'_{\rm d}(t_l)\rangle + |\Delta\Psi_{\rm d}(t_l)\rangle - |\Delta\Psi_{\rm r}(t_l)\rangle, \qquad (30)$$

$$|\Psi_{\rm r}(t_l)\rangle = |\Psi'_{\rm r}(t_l)\rangle + |\Delta\Psi_{\rm r}(t_l)\rangle. \qquad (31)$$

By this algorithm, the sum of the components $|\Psi_{\rm ion}(t_l)\rangle$, $|\Psi_{\rm d}(t_l)\rangle$, and $|\Psi_{\rm r}(t_l)\rangle$ satisfies the same initial condition as $|\Psi_{\rm L}(t_l)\rangle$ at $t = t_{\rm i}$ and follows the same evolution as Eq. (17). Therefore, at each t_l, the following relation for the exact decomposition is guaranteed:

$$|\Psi_{\rm L}(t_l)\rangle = |\Psi_{\rm ion}(t_l)\rangle + |\Psi_{\rm d}(t_l)\rangle + |\Psi_{\rm r}(t_l)\rangle. \quad (32)$$

At the end of simulations, the PMDs $|\tilde{\Psi}_{\rm d}(\mathbf{p})|^2$ and $|\tilde{\Psi}_{\rm r}(\mathbf{p})|^2$ for direct and rescattering ionization were obtained by Fourier transforming $\Psi_{\rm d}(x,y,t_{\rm f})$ and $\Psi_{\rm r}(x,y,t_{\rm f})$, respectively.

III. RESULTS AND DISCUSSION

A. Effect of the long-range part of the Coulomb potential

Figure 1 shows the PMDs of H [Figs. 1(a)–1(f)] and H_2^+ [Figs. 1(g)–1(l)] obtained with different screened Coulomb potentials. We set the laser intensity at 1×10^{14} W/cm^2 and the wavelength at 800 nm. The laser electric field rotates clockwise. For Figs. 1(a) and 1(g) we completely neglected the Coulomb interaction between the liberated electron and the parent core by removing the Coulomb potential in $\bar{U}$ in Eq. (13). As expected by the SFA, the PMDs in Figs. 1(a) and 1(g) are peaked in the $+p_y$ and $-p_y$ directions, i.e., perpendicular to the major polarization axis and the molecular axis, respectively. The PMDs are asymmetric between the $+p_y$ and $-p_y$ directions because a few-cycle laser pulse is applied in the present simulations. From Fig. 1(b) to Fig. 1(f) we increased the cutoff radius r_0 of the screened Coulomb potential $V_{\rm SC}(x,y;r_0)$ in Eq. (19) from 2 to 100 a.u. for the H atom. Similarly, from Fig. 1(h) to Fig. 1(l) we increased r_0 from 3 to 100 a.u. for H_2^+. As r_0 increases, the PMD rotates away from the directions expected by the SFA. Between $r_0 = 15$ and 100 a.u., the PMDs show only a small difference for both H [cf. Figs. 1(e) and 1(f)] and H_2^+ [cf. Figs. 1(k) and 1(l)]. These results clearly demonstrate that, for the given laser parameters, the Coulomb tail in the range of 10–15 a.u. plays an essential role in the rotation of the PMD in both atomic and molecular systems. This supports the similar conclusion that the Coulomb interaction near the parent ion right after the tunneling distorts the PMD from the SFA prediction, derived with different approaches [34,36,38,41,47,49,50]. In the rest of this paper we use the unscreened Coulomb potential $V_{\rm C}$ and focus on the difference of the ionization dynamics between atomic and molecular systems. To quantify the PMDs in the laser polarization plane, we define an angle θ, as shown in Fig. 1(l). The value of θ is positive if the PMD rotates clockwise away from the p_y axis.

B. Direct and rescattering ionization

The PMD for H_2^+ in Fig. 1(l) shows additional weaker peaks at $\theta \approx 80^\circ$ and 260° compared to the PMD for H in Fig. 1(f). We propose the explanation that these peaks are attributed to rescattering processes. The rescattering event is known to be significantly suppressed as the ellipticity of the laser field is changed from linear polarization to circular polarization for atoms [79–81] unless a specific condition is met [82]. However, in molecular systems, an electron wave packet released from one nucleus may be rescattered by another nucleus even in a circularly polarized laser field [83].

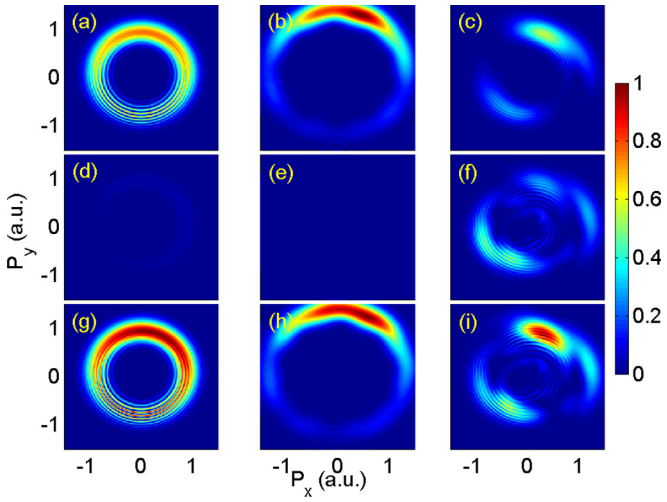

FIG. 3. (Color online) The PMDs of (a)–(c) direct ionization $|\tilde{\Psi}_{\rm d}(\mathbf{p})|^2$, (d)–(f) rescattering ionization $|\tilde{\Psi}_{\rm r}(\mathbf{p})|^2$, and (g)–(i) full ionization $|\tilde{\Psi}_{\rm d}(\mathbf{p}) + \tilde{\Psi}_r(\mathbf{p})|^2$ of (a), (d), and (g) H, (b), (e), and (h) H_2^+ at internuclear distance 2 a.u., and (c), (f), and (i) H_2^+ at internuclear distance 5 a.u. The laser pulse has the wavelength 800 nm and the intensities (a), (d), and (g) 10^{14} W/cm^2, (b), (e), and (h) 1.42×10^{14} W/cm^2, and (c), (f), and (i) 10^{14} W/cm^2. The PMDs are normalized so that the maximum values in (g)–(i) are equal to unity.

We examined our proposition by using the method described in Sec. II D to disentangle the ionized wave packet into the direct and rescattered components. Figure 3 shows the PMD $|\tilde{\Psi}_{\rm d}(\mathbf{p})|^2$ of the direct ionization components [Figs. 3(a)–3(c)], the PMD $|\tilde{\Psi}_{\rm r}(\mathbf{p})|^2$ of the rescattering components [Figs. 3(d)–3(f)], and the coherent sum $|\tilde{\Psi}_{\rm d}(\mathbf{p}) + \tilde{\Psi}_{\rm r}(\mathbf{p})|^2$ of the direct and rescattering components [Figs. 3(g)–3(i)] when the internuclear distances of H_2^+ are 2 a.u. [Figs. 3(b), 3(e), and 3(h)] and 5 a.u. [Figs. 3(c), 3(f), and 3(i)], respectively. For comparison, we show the corresponding PMD of H in Figs. 3(a), 3(d), and 3(g). We set $r_{\rm d} = 8$ a.u. and $r_{\rm s} = 5$ a.u. for the decomposition, and the small changes of $r_{\rm d}$ and $r_{\rm s}$ did not change these PMDs sensitively. We have tested that the coherent sum recovers the full PMD $|\tilde{\Psi}(\mathbf{p})|$ of the total ionization signal obtained by propagating the full wave packet without such decomposition. This confirms that the contribution of the component $|\Psi_{\rm ion}(t_l)\rangle$ in Eq. (32) becomes negligibly small by the end of the simulation at $t = t_{\rm f}$ and also validates our decomposition method. When the internuclear distances of H_2^+ are 2 and 5 a.u., the ionization potentials are 1.05 and 0.74 a.u. Note that the ionization of H_2^+ is between tunneling and multiphoton regimes when the intensity is 10^{14} W/cm^2 for $R = 2$ a.u. Therefore we apply the laser intensities 1.42×10^{14} and 10^{14} W/cm^2 for cases $R = 2$ and 5 a.u., respectively, to keep the Keldysh parameters the same and to trigger tunneling ionization in both cases. The laser intensity applied in H is still 10^{14} W/cm^2, the same as that in Fig. 1.

When the internuclear distance is 2 a.u., the spatial extent of the Coulomb potential is closer to the hydrogen atomic potential. Hence, the rescattering hardly happens when the circularly polarized laser pulse is applied, as shown in Fig. 3(e).

However, when the internuclear distance is 5 a.u., the Coulomb potential extends to a relatively large area, and the electron emitted from one nucleus may collide with another nucleus, presenting a rescattering feature. Figures 3(c), 3(f), and 3(i) clearly show that the main peaks at around $\theta = 30^\circ$ are mainly contributed by the direct ionization, whereas the rescattered wave packet has the contribution at a larger θ angle and higher absolute value of momenta than the direct ionization. This observation also is in accord with the expectation that the Coulomb potential has a stronger effect on the rescattering ionization than direct ionization because the Coulomb potential plays a role in both tunneling and rescattering processes [83]. We note, however, that this rescattering feature may be overestimated in the present 2D model and may not be well recognized in the experimental data [44,45] and the simulation results of classical 3D model [46] because the wave packet can spread out of the laser polarization plane to some extent in the actual 3D system.

C. Dependence of the drift angle on the laser intensity and wavelength

After investigating the Coulomb interaction, we now turn our attention to the other potential term in the Hamiltonian, i.e., the laser-electron interaction expressed by Eq. (3). Figure 4(a) shows the drift angle as a function of the laser wavelength and intensity for H_2^+, where the drift angle is defined as the angle giving the maximum angular probability density (obtained by integrating the 2D PMD over the radial momentum) measured from the p_y axis. The result shows an overall propensity that

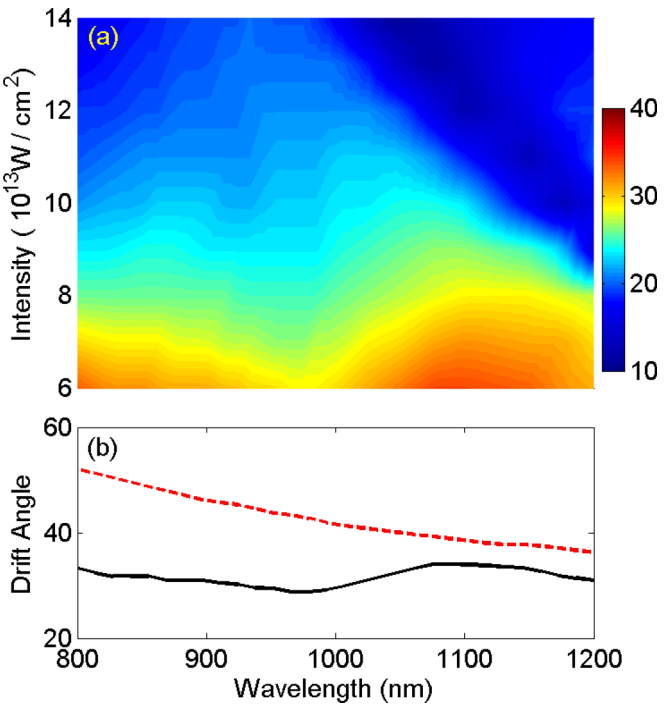

FIG. 4. (Color online) (a) Drift angle as a function of laser wavelengths and intensities. (b) The cut of (a) at a laser intensity 6×10^{13} W/cm^2 (black solid line). For reference, the drift angle of the PMD for H is shown by the red dashed curve when the same laser parameters are applied.

the drift angle decreases as the laser wavelength and intensity increase. This propensity may be understood in terms of the classical motion of the released electron in the laser field. The electron would gain momentum proportional to E_0/ω from the laser field and would trace a cycloid trajectory of radius E_0/ω^2 in the absence of the Coulomb potential. Therefore, as the laser intensity and/or the wavelength increase, we may deduce that the electron moves away from the parent ion more quickly in an orbit with a larger radius. As a result, the Coulomb interaction between the electron and the parent ion is reduced while the laser-electron interaction dominates the evolution of the released electron. We consider that for a higher intensity and longer wavelength, the SQC model and the SFA, both of which neglect the electron-ion Coulomb interaction, work better in describing the PMD. The overall propensity agrees with the previously reported experimental data and simulation results about the dependence on laser intensities [38,40,41,47,50] and wavelengths [46,83]. However, we note that a few other previous theoretical studies have reported that the drift angle increases with higher intensity, which has been explained as a result of the tunnel exit point moving closer to the parent ion in a higher-intensity laser field [41,49]. To assess consistency among the results obtained at somewhat different physical conditions, further studies will be needed.

In addition to the overall trend described above, our fine-interval systematic simulations reveal in Fig. 4(a) an oscillatory structure in the drift angle as a function of the laser intensity and wavelength. We extracted the dependence of the drift angle on the wavelength at the intensity 6×10^{13} W/cm^2 as the black solid curve shown in Fig. 4(b). As a reference, we also present by the red dashed curve the drift angle of the PMD for the H atom calculated at the same laser intensity and the ellipticity $\epsilon = 0.6$. In the atomic case, the drift angle decreases monotonically for longer wavelengths, in contrast to the molecular case.

To explore the origin of the nonmonotonic dependence in the molecular case, we look into the time-dependent ionization rate $-[\frac{d}{dt}P_{\text{bound}}(t)]/P_{\text{bound}}(t)$ for H and H_2^+. We define the bound population $P_{\text{bound}}(t)$ as the probability for the electron to be within the radius $r_{\text{bound}} = 30$ a.u. from the center of the parent ion. Figures 5(a) and 5(b) show the ionization rates for H and H_2^+, respectively, as a function of time at three different laser wavelengths, 800, 1000, and 1100 nm. For the case of H, one can see peaks separated in time by about $T/2$, and these peaks may be interpreted as the electron being released mainly when $|\mathbf{E}(t)|$ of the EP laser field is maximized in each half cycle in accordance with the QSTI picture. The ionization rate of H_2^+ also shows peaks separated by a half cycle, but some peaks show finer structures (e.g., splitting into small peaks around $t = 0.8T$ and $1.0T$ for the 800-nm wavelength), which may indicate that the electron is released from the molecule multiple times in a half cycle [44,67].

The peaks of the ionization rate in Fig. 5(a) do not appear exactly at the instants when the electric field is maximum (i.e., $t = 0, \pm T/2, \ldots$). This is because the electron emitted from the nucleus takes some time to travel to the region $r > r_{\text{bound}}$. Such delays exist in Fig. 5(b) as well, and the traveling delay should also depend on the laser parameters as we can see that the peaks move in time slightly in Figs. 5(a) and 5(b). However, we may assume here that the free-electron

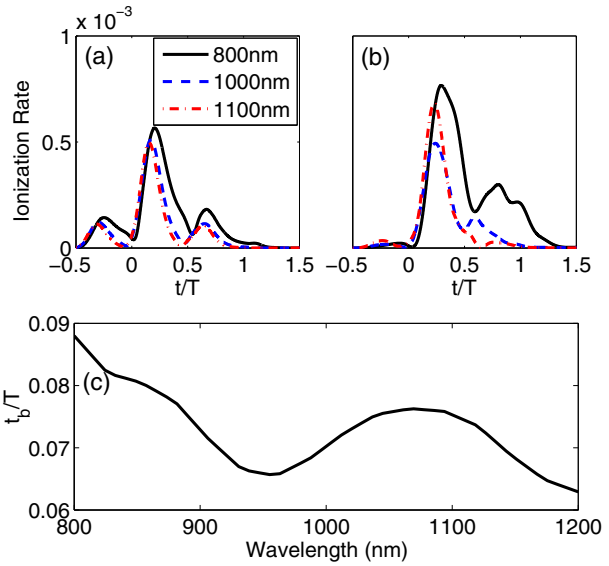

FIG. 5. (Color online) Time-dependent ionization rate for (a) H and (b) H_2^+. (c) Photoelectron emission timing t_b of H_2^+ as a function of laser wavelengths. The laser intensity was 6×10^{13} W/cm^2. See the text for the calculation of t_b.

traveling time in the H and H_2^+ cases are the same under the same laser conditions. Then, by subtracting the moment giving the highest peaks in Fig. 5(a) from that in Fig. 5(b), we can exclude the traveling time and precisely determine the relative timing t_b at which the electron leaves the nuclei of H_2^+ compared to H. Figure 5(c) shows the dependence of t_b on the wavelength. We can see that t_b/T fluctuates with the laser wavelength. The marked resemblance between the wavelength dependence of the drift angle in Fig. 4(b) (black solid curve) and the relative ionization time t_b/T in Fig. 5(c) suggests that the nonmonotonic wavelength dependence of the drift angle in H_2^+ originates from the fluctuation of the ionization timing. That is, the electron is emitted at different phases of electric field and therefore accelerates in different directions, depending on the wavelength. The minimization of the drift angle at the 980-nm wavelength may be explained by the relative ionization timing being most advanced at this laser condition. This interpretation is also consistent with the previous reports that the emission timing influences the PMD rotation in H_2^+ [44,46].

The fluctuation of the ionization instant is due to the transient electron localization in H_2^+. Though the laser-H_2^+ coupling is strongest at $t = 0$, the largest ionization rate may not happen at $t = 0$ due to the electron localization. When H_2^+ is exposed to strong laser fields, the electron hops between two nuclei. It was demonstrated that the electron leaves the molecule from the uphill potential well [68]. Depending on the laser wavelength (and other laser parameters), the electron localizes to the uphill well at different timings, and hence the timing of the electron release is also expected to fluctuate.

D. Connection to other parameter regimes

We have compared the PMD rotation between atomic and molecular systems in the simplest settings. Before concluding, we discuss briefly the PMD in some other regimes of system parameters.

One interesting point to be examined is how general the mechanism of PMD rotation is over the tunneling and multiphoton ionization regimes. The rotation of the PMD has been predicted at the XUV [51,53] and visible [52] laser wavelengths as well. As the wavelength becomes shorter (while keeping the intensity constant at around 10^{14} W/cm^2), the number of absorbed photons decreases, and the PMD can be analyzed by the conventional weak-field perturbation theory in the XUV range [51]. In both short- and long-wavelength regimes, the Coulomb interaction between the core and the liberated electron is considered to influence the PMD rotation [51–53]. However, as the photon energy of the ionizing laser field increases, the transient electron localization will have a diminished effect with less population transferred between H_2^+ nuclei [84]. Also, we may no longer picture the electron as slowly tunneling out from the binding potential and being accelerated while spiraling away from the core, which has been the basis of some of the calculations taking into account the Coulomb effect perturbatively on the classical trajectories [30,36,38,41]. Rather, a representation in terms of a small number of partial waves (whose quantization axis is rotated from the symmetry axis of the system) may possibly be more suitable for the electronic wave packet in the XUV laser field. A theory that can connect the two wavelength regimes and explain the persistence or switching of mechanisms of the PMD rotation still needs to be worked out. In the XUV range, one of the motivations to study the PMD is to retrieve the electronic states of a molecule under the field-free condition [51,53]. In contrast, in the IR range, we may potentially read out the laser-driven electron dynamics from the PMD if we can develop an accurate theory to reconstruct the PMD.

A clear difference between the tunneling ionization and the single-XUV-photon ionization is that the drift angle does not depend on the laser intensity in the latter case [51]. In the single-XUV-photon ionization, the ionized electron acquires the intensity-independent velocity $\sqrt{2(\omega_{\mathrm{XUV}} - I_{\mathrm{p}})}$, where ω_{XUV} is the angular frequency of the XUV laser field, and I_{p} is the ionization potential of an atom or molecule. Therefore, the Coulomb effect on the photoelectron is independent of the XUV intensity. In contrast, in the case of the tunneling ionization, the freed electron has a velocity proportional to the laser field. In a higher-intensity laser field, the freed electron will be accelerated more and leaves the nucleus more quickly, hence the Coulomb effect on the freed electron is weaker, resulting in an overall smaller drift angle.

Another important point to be studied carefully in the molecular case is the dependence of the rotation of the PMD on the geometry of the system, i.e., internuclear distance for diatomic molecules and more generally the skeletal structure of polyatomic molecules, and the orientation of the molecule with respect to the laboratory frame defined by the laser field, as well as the ellipticity of the laser field. Peters *et al.* have reported that the electron diffraction is very sensitive to molecular alignments [85].

As a first step of *ab initio* numerical simulation toward a more complex geometry, we calculated the PMDs from the 2D model of H_2^+ in an EP laser field. Figure 6 shows the PMDs when the internuclear axis is aligned at the angles 0

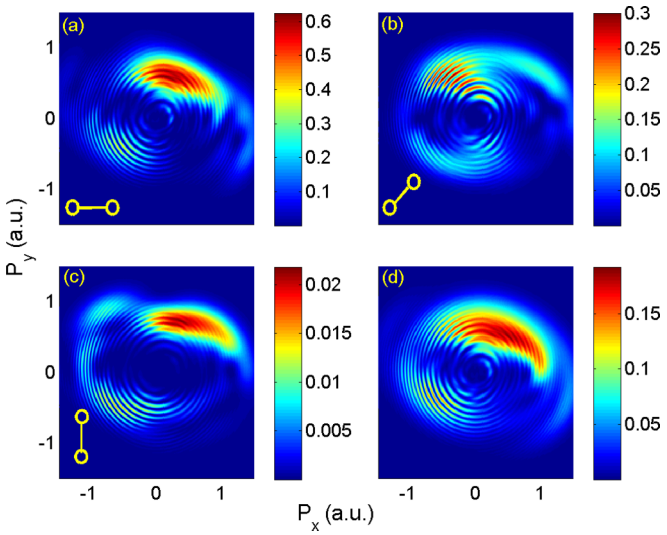

FIG. 6. (Color online) The PMD from H_2^+ aligned at the angles (a) 0, (b) $\pi/4$, and (c) $\pi/2$ from the major polarization axis. (d) Statistical average of the PMD assuming H_2^+ is randomly aligned in the laser polarization plane. The internuclear distance is fixed at $R = 5$ a.u., the ellipticity of the laser field is $\epsilon = 0.6$, and the laser intensity is 1×10^{14} W/cm^2.

[Fig. 6(a)], $\pi/4$ [Fig. 6(b)], and $\pi/2$ [Fig. 6(c)] with respect to the major axis of polarization ellipse, which is set along the x axis. The tunneling and rescattering processes depend on the molecular alignment since the Coulomb potential is anisotropic, and this is reflected in the PMDs. We note that in the single-XUV-photon ionization, the drift angle does not seem to depend on the molecular alignment [51]. Figure 6(d) shows the statistically averaged PMDs obtained by incoherently adding the PMDs at different alignment for a randomly oriented molecular ensemble. Note that the color bars in the respective panels of Fig. 6 have different scales. By comparing Figs. 6(a) and 6(d), one may conclude that the ionization is mainly contributed by the molecules aligned parallel to the major polarization axis. Previously, with a modified version of the SFA, the photoelectron momentum angular distribution was calculated for a diatomic molecule at several three-dimensional orientations in an EP laser field [69]. The angular distributions reported therein were all much sharper than the PMDs in Fig. 6, even though the two results cannot be directly compared because of the difference of the laser and molecular parameters as well as the dimensionality of the model. This gap needs to be filled with more comprehensive theory and to be tested against experimental data. For molecules oriented out of the plane of laser polarization [69], it would also be interesting to check whether and how the PMDs in the lateral direction [72,86,87] with respect to the polarization plane are coupled to the PMDs on the polarization plane.

The molecular structure can influence the PMDs in at least two ways. First, the rescattering effect may be stronger for larger internuclear distance (see Fig. 3). Second, the intramolecular electron dynamics prior to ionization is also influenced by the internuclear distance of diatomic molecules [65–67,84]. For polyatomic aromatic molecules, the ring current may also be influenced by the static structure and dynamical change thereof (i.e., vibration) [70,71]. These electron dynamics inside the molecule can modify the PMDs as we discussed in Sec. III C. In passing, a very recent theoretical study revealed that not only H_2^+ but also the H atom as well as a heteronuclear diatomic molecule can show multiple peaks of ionization within half a cycle in linearly polarized light [88]. It is left for future study whether these multiple-ionization bursts remain in an EP laser field and if so whether the timings of ionization have the same influence on the angular drift of the PMD as H_2^+.

Finally, multielectron effects on the PMD rotation must also be understood in a complex molecule. It has already been pointed out that the Coulomb interaction between the cation core and the liberated electron is partially shielded by the bound electrons' polarization induced by the laser field [30,38,41,50]. In addition, in multielectron systems, an electron can be released not only from the highest-occupied orbital but also from lower-lying orbitals [89,90], and these multiple orbitals coherently contribute to the PMD. Furthermore, the electron-electron correlation in the initial state [53], as well as that generated by recollision in nonsequential double ionization [82], and through the emission timings in sequential double ionization [91–94] may also influence the PMD rotation. While the first effect (i.e., the polarization effect) has been taken into account in the theoretical treatment based on classical trajectories [30,38,41,50], the latter two effects (multiorbital effect and correlation effect) on the PMD have rarely been analyzed. In fact, it is interesting that the electron from the first ionization of neutral H_2 by a circularly polarized laser field shows little rotation in the PMD, and that the electron from the second ionization shows a significant rotation [47,95,96]. The residual charge of the core may explain this to some extent but not completely, because a significant rotation has been observed from neutral atoms in the EP laser field [31,34,38]. At the moment, it is impractical to simulate the two or more electrons fully quantum mechanically in 3D space under an IR laser field, and the first systematic analysis of these effects may need to be carried out with methods that utilize classical mechanics effectively [63,82].

The photoionization process may seem elementary and well understood over the many years of study. However, as we discussed here, there are still many unknown aspects, the understanding of which may lead to new methods for measurement and control of the attosecond electron dynamics in atoms and molecules.

IV. CONCLUSION

In summary, we studied the PMDs of H in an EP laser field and of H_2^+ in a CP laser field with 2D quantum-mechanical models. By screening the interaction between the free electron and the parent ion at a systematically changed cutoff radius, we demonstrated that the Coulomb interaction in the range of 10–15 a.u. from the center of the parent ion is essential for explaining the angular deviation of the PMD from the expectation of the SQC model and the SFA. By decomposing the wave packet into direct and rescattered components in the H_2^+ model, we identified that the weaker peaks at larger drift angle and higher radial momentum seen in our 2D model are

mainly contributed by rescattered components. By calculating the drift angle of the PMD for H_2^+ as a function of the laser intensity and wavelength, we found the overall trend that the drift angle decreases as the intensity increases and as the wavelength increases. We found that the drift angle depends nonmonotonically on wavelengths for H_2^+ in contrast to the monotonic dependence for H atom. By comparing the time-resolved ionization rates of H_2^+ and H, we saw that the timing of electron emission from H_2^+ fluctuates with respect to that from the H atom as the laser wavelength changes, and that this fluctuation can explain the nonmonotonic dependence of the drift angle on the laser wavelength.

ACKNOWLEDGMENTS

This work was supported by NSF of China (Grants No. 11104180, No. 11175120, No. 11121504, and No. 11322438) and the Fok Ying-Tong Education Foundation for Young Teachers in the Higher Education Institutions of China (Grant No. 131010).

[1] T. Wittmann, B. Horvath, W. Helml, M. G. Schätzel, X. Gu, A. L. Cavalieri, G. G. Paulus, and R. Kienberger, Nat. Phys. **5**, 357 (2009).
[2] J. Itatani, F. Quéré, G. L. Yudin, M. Y. Ivanov, F. Krausz, and P. B. Corkum, Phys. Rev. Lett. **88**, 173903 (2002).
[3] M. Kitzler, N. Milosevic, A. Scrinzi, F. Krausz, and T. Brabec, Phys. Rev. Lett. **88**, 173904 (2002).
[4] E. Goulielmakis, M. Uiberacker, R. Kienberger, A. Baltuska, V. Yakovlev, A. Scrinzi, T. Westerwalbesloh, U. Kleineberg, U. Heinzmann, M. Drescher *et al.*, Science **305**, 1267 (2004).
[5] P. Eckle, M. Smolarski, P. Schlup, J. Biegert, A. Staudte, M. Schöffler, H. G. Muller, R. Dörner, and U. Keller, Nat. Phys. **4**, 565 (2008).
[6] T. Morishita, A.-T. Le, Z. Chen, and C. D. Lin, Phys. Rev. Lett. **100**, 013903 (2008).
[7] C. D. Lin, A.-T. Le, Z. Chen, T. Morishita, and R. Lucchese, J. Phys. B **43**, 122001 (2010).
[8] J. Itatani, J. Levesque, D. Zeidler, H. Niikura, H. Pépin, J. C. Kieffer, P. B. Corkum, and D. M. Villeneuve, Nature (London) **432**, 867 (2004).
[9] M. Lein, J. Phys. B **40**, R135 (2007).
[10] F. Krausz and M. Ivanov, Rev. Mod. Phys. **81**, 163 (2009).
[11] L. D. Landau and E. M. Lifshitz, *Quantum Mechanics: Non-Relativistic Theory*, 3rd ed. (Pergamon, Oxford, 1977), Sec. 77.
[12] M. V. Ammosov, N. B. Delone, and V. P. Krănov, Zh. Eksp. Teor. Fiz. **91**, 2008 (1986) [Sov. Phys. JETP **64**, 1191 (1986)].
[13] N. B. Delone and V. P. Krainov, J. Opt. Soc. Am. B **8**, 1207 (1991).
[14] X. M. Tong, Z. X. Zhao, and C. D. Lin, Phys. Rev. A **66**, 033402 (2002).
[15] H. B. van Linden van den Heuvell and H. G. Muller, in *Multiphoton Processes*, edited by S. J. Smith and P. L. Knight (Cambridge University Press, Cambridge, 1988), pp. 25–35.
[16] P. B. Corkum, Phys. Rev. Lett. **71**, 1994 (1993).
[17] J. L. Krause, K. J. Schafer, and K. C. Kulander, Phys. Rev. Lett. **68**, 3535 (1992).
[18] L. Keldysh, Zh. Eksp. Teor. Fiz. **47**, 1945 (1964) [Sov. Phys. JETP **20**, 1307 (1965)].
[19] F. H. M. Faisal, J. Phys. B **6**, L89 (1973).
[20] H. R. Reiss, Phys. Rev. A **22**, 1786 (1980).
[21] A. Becker and F. Faisal, J. Phys. B **38**, R1 (2005).
[22] D. B. Milošević, G. G. Paulus, D. Bauer, and W. Becker, J. Phys. B **39**, R203 (2006).
[23] A. Becker and F. H. M. Faisal, Phys. Rev. Lett. **89**, 193003 (2002).
[24] D. G. Arbó, J. E. Miraglia, M. S. Gravielle, K. Schiessl, E. Persson, and J. Burgdörfer, Phys. Rev. A **77**, 013401 (2008).
[25] M. Ciappina and W. Cravero, J. Mod. Opt. **56**, 11 (2009).
[26] C. I. Blaga, F. Catoire, P. Colosimo, G. G. Paulus, H. G. Muller, P. Agostini, and L. F. DiMauro, Nat. Phys. **5**, 335 (2009).
[27] W. Quan, Z. Lin, M. Wu, H. Kang, H. Liu, X. Liu, J. Chen, J. Liu, X. T. He, S. G. Chen *et al.*, Phys. Rev. Lett. **103**, 093001 (2009).
[28] T.-M. Yan, S. V. Popruzhenko, M. J. J. Vrakking, and D. Bauer, Phys. Rev. Lett. **105**, 253002 (2010).
[29] A. Kästner, U. Saalmann, and J. M. Rost, J. Phys. B **45**, 074011 (2012).
[30] D. Dimitrovski, J. Maurer, H. Stapelfeldt, and L. B. Madsen, Phys. Rev. Lett. **113**, 103005 (2014).
[31] M. Bashkansky, P. H. Bucksbaum, and D. W. Schumacher, Phys. Rev. Lett. **60**, 2458 (1988).
[32] F. Trombetta, G. Ferrante, and S. Basile, J. Phys. B **21**, L539 (1988).
[33] S. Basile, F. Trombetta, and G. Ferrante, Phys. Rev. Lett. **61**, 2435 (1988).
[34] S. P. Goreslavski, G. G. Paulus, S. V. Popruzhenko, and N. I. Shvetsov-Shilovski, Phys. Rev. Lett. **93**, 233002 (2004).
[35] A. Jaroń, J. Kamiński, and F. Ehlotzky, Opt. Commun. **163**, 115 (1999).
[36] M. Li, Y. Liu, H. Liu, Q. Ning, L. Fu, J. Liu, Y. Deng, C. Wu, L.-Y. Peng, and Q. Gong, Phys. Rev. Lett. **111**, 023006 (2013).
[37] P. Eckle, A. N. Pfeiffer, C. Cirelli, A. Staudte, R. Dörner, H. G. Muller, M. Büttiker, and U. Keller, Science **322**, 1525 (2008).
[38] A. N. Pfeiffer, C. Cirelli, M. Smolarski, D. Dimitrovski, M. Abu-samha, L. B. Madsen, and U. Keller, Nat. Phys. **8**, 76 (2012).
[39] D. Shafir, H. Soifer, C. Vozzi, A. S. Johnson, A. Hartung, Z. Dube, D. M. Villeneuve, P. B. Corkum, N. Dudovich, and A. Staudte, Phys. Rev. Lett. **111**, 023005 (2013).
[40] C. P. J. Martiny, M. Abu-samha, and L. B. Madsen, J. Phys. B **42**, 161001 (2009).
[41] N. I. Shvetsov-Shilovski, D. Dimitrovski, and L. B. Madsen, Phys. Rev. A **85**, 023428 (2012).
[42] P. Krstić and M. H. Mittleman, Phys. Rev. A **44**, 5938 (1991).
[43] A. S. Landsman, C. Hofmann, A. N. Pfeiffer, C. Cirelli, and U. Keller, Phys. Rev. Lett. **111**, 263001 (2013).
[44] M. Odenweller, N. Takemoto, A. Vredenborg, K. Cole, K. Pahl, J. Titze, L. P. H. Schmidt, T. Jahnke, R. Dörner, and A. Becker, Phys. Rev. Lett. **107**, 143004 (2011).

[45] M. Odenweller, J. Lower, K. Pahl, M. Schütt, J. Wu, K. Cole, A. Vredenborg, L. P. Schmidt, N. Neumann, J. Titze *et al.*, Phys. Rev. A **89**, 013424 (2014).

[46] C. Huang, Z. Li, Y. Zhou, Q. Tang, Q. Liao, and P. Lu, Opt. Express **20**, 11700 (2012).

[47] M. Spanner, S. Gräfe, S. Chelkowski, D. Pavičić, M. Meckel, D. Zeidler, A. B. Bardon, B. Ulrich, A. D. Bandrauk, D. M. Villeneuve *et al.*, J. Phys. B **45**, 194011 (2012).

[48] J. Wu, M. Meckel, S. Voss, H. Sann, M. Kunitski, L. P. H. Schmidt, A. Czasch, H. Kim, T. Jahnke, and R. Dörner, Phys. Rev. Lett. **108**, 043002 (2012).

[49] K. Doblhoff-Dier, K. I. Dimitriou, A. Staudte, and S. Gräfe, Phys. Rev. A **88**, 033411 (2013).

[50] J. Maurer, D. Dimitrovski, L. Christensen, L. B. Madsen, and H. Stapelfeldt, Phys. Rev. Lett. **109**, 123001 (2012).

[51] K.-J. Yuan, S. Chelkowski, and A. D. Bandrauk, J. Chem. Phys. **138**, 134316 (2013).

[52] K.-J. Yuan and A. D. Bandrauk, Phys. Rev. A **84**, 013426 (2011).

[53] K.-J. Yuan and A. D. Bandrauk, Phys. Rev. A **85**, 053419 (2012).

[54] F. Lindner, M. G. Schätzel, H. Walther, A. Baltuška, E. Goulielmakis, F. Krausz, D. B. Milošević, D. Bauer, W. Becker, and G. G. Paulus, Phys. Rev. Lett. **95**, 040401 (2005).

[55] A. Picón, A. Bahabad, H. C. Kapteyn, M. M. Murnane, and A. Becker, Phys. Rev. A **83**, 013414 (2011).

[56] I. V. Litvinyuk, K. F. Lee, P. W. Dooley, D. M. Rayner, D. M. Villeneuve, and P. B. Corkum, Phys. Rev. Lett. **90**, 233003 (2003).

[57] M. Plummer and J. McCann, J. Phys. B **30**, L401 (1997).

[58] D. Pavičić, A. Kiess, T. W. Hänsch, and H. Figger, Phys. Rev. Lett. **94**, 163002 (2005).

[59] M. Lezius, S. Dobosz, D. Normand, and M. Schmidt, Phys. Rev. Lett. **80**, 261 (1998).

[60] T. Ergler, A. Rudenko, B. Feuerstein, K. Zrost, C. D. Schröter, R. Moshammer, and J. Ullrich, Phys. Rev. Lett. **97**, 193001 (2006).

[61] X. Xie, K. Doblhoff-Dier, S. Roither, M. S. Schöffler, D. Kartashov, H. Xu, T. Rathje, G. G. Paulus, A. Baltuška, S. Gräfe *et al.*, Phys. Rev. Lett. **109**, 243001 (2012).

[62] R. E. F. Silva, F. Catoire, P. Rivière, H. Bachau, and F. Martín, Phys. Rev. Lett. **110**, 113001 (2013).

[63] E. Lötstedt, T. Kato, and K. Yamanouchi, Phys. Rev. Lett. **106**, 203001 (2011).

[64] T. Zuo and A. D. Bandrauk, Phys. Rev. A **52**, R2511 (1995).

[65] I. Kawata, H. Kono, and Y. Fujimura, J. Chem. Phys. **110**, 11152 (1999).

[66] F. He, A. Becker, and U. Thumm, Phys. Rev. Lett. **101**, 213002 (2008).

[67] N. Takemoto and A. Becker, Phys. Rev. Lett. **105**, 203004 (2010).

[68] J. Wu, M. Magrakvelidze, L. Schmidt, M. Kunitski, T. Pfeifer, M. Schöffler, M. Pitzer, M. Richter, S. Voss, H. Sann *et al.*, Nat. Commun. **4**, 2177 (2013).

[69] M. Busuladžić, A. Gazibegović-Busuladžić, and D. B. Milošević, Phys. Rev. A **80**, 013420 (2009).

[70] I. Barth, J. Manz, Y. Shigeta, and K. Yagi, J. Am. Chem. Soc. **128**, 7043 (2006).

[71] M. Kanno, H. Kono, Y. Fujimura, and S. H. Lin, Phys. Rev. Lett. **104**, 108302 (2010).

[72] L. Arissian, C. Smeenk, F. Turner, C. Trallero, A. V. Sokolov, D. M. Villeneuve, A. Staudte, and P. B. Corkum, Phys. Rev. Lett. **105**, 133002 (2010).

[73] X. M. Tong, K. Hino, and N. Toshima, Phys. Rev. A **74**, 031405(R) (2006).

[74] X. M. Tong, S. Watahiki, K. Hino, and N. Toshima, Phys. Rev. Lett. **99**, 093001 (2007).

[75] M. Y. Ivanov, M. Spanner, and O. Smirnova, J. Mod. Opt. **52**, 165 (2005).

[76] M. D. Feit, J. A. Fleck, Jr., and A. Steiger, J. Comput. Phys. **47**, 412 (1982).

[77] C. C. Marston and G. G. Balint-Kurti, J. Chem. Phys. **91**, 3571 (1989).

[78] A. D. Bandrauk and H. Shen, J. Chem. Phys. **99**, 1185 (1993).

[79] P. Krstić and M. H. Mittleman, Phys. Rev. Lett. **103**, 103007 (2009).

[80] W. A. Bryan, S. L. Stebbings, J. McKenna, E. M. L. English, M. Suresh, J. Wood, B. Srigengan, I. C. E. Turcu, J. M. Smith, E. J. Divall *et al.*, Nat. Phys. **2**, 379 (2006).

[81] F. He, C. Ruiz, and A. Becker, Opt. Lett. **32**, 3224 (2007).

[82] F. Mauger, C. Chandre, and T. Uzer, Phys. Rev. Lett. **105**, 083002 (2010).

[83] W. Yang, Z. Sheng, X. Feng, M. Wu, Z. Chen, and X. Song, Opt. Express **22**, 2519 (2014).

[84] N. Takemoto and A. Becker, Phys. Rev. A **84**, 023401 (2011).

[85] M. Peters, T. T. Nguyen-Dang, E. Charron, A. Keller, and O. Atabek, Phys. Rev. A **85**, 053417 (2012).

[86] D. Dimitrovski, C. P. J. Martiny, and L. B. Madsen, Phys. Rev. A **82**, 053404 (2010).

[87] J. Henkel, M. Lein, V. Engel, and I. Dreissigacker, Phys. Rev. A **85**, 021402(R) (2012).

[88] D. A. Telnov, K. Nasiri Avanaki, and S.-I. Chu, Phys. Rev. A **90**, 043404 (2014).

[89] H. Akagi, T. Otobe, A. Staudte, A. Shiner, F. Turner, R. Dörner, D. M. Villeneuve, and P. B. Corkum, Science **325**, 1364 (2009).

[90] X. Gong, Q. Song, Q. Ji, H. Pan, J. Ding, J. Wu, and H. Zeng, Phys. Rev. Lett. **112**, 243001 (2014).

[91] X. Wang, J. Tian, and J. H. Eberly, Phys. Rev. Lett. **110**, 073001 (2013).

[92] A. Tong, Y. Zhou, C. Huang, and P. Lu, J. Chem. Phys. **139**, 074308 (2013).

[93] A. N. Pfeiffer, C. Cirelli, M. Smolarski, R. Dörner, and U. Keller, Nat. Phys. **7**, 428 (2011).

[94] Y. Zhou, C. Huang, Q. Liao, and P. Lu, Phys. Rev. Lett. **109**, 053004 (2012).

[95] A. Staudte, S. Patchkovskii, D. Pavičić, H. Akagi, O. Smirnova, D. Zeidler, M. Meckel, D. M. Villeneuve, R. Dörner, M. Y. Ivanov *et al.*, Phys. Rev. Lett. **102**, 033004 (2009).

[96] M. Magrakvelidze, F. He, S. De, I. Bocharova, D. Ray, U. Thumm, and I. V. Litvinyuk, Phys. Rev. A **79**, 033408 (2009).